

YU.M. LYASCHUK, V.V. KOROTYHEYEV

V.E. Lashkaryov Institute of Semiconductor Physics, Nat. Acad. of Sci. of Ukraine
(41, Nauky Ave., Kyiv 03028, Ukraine; e-mail: korotcev@ukr.net)

INTERACTION OF A TERAHERTZ ELECTROMAGNETIC WAVE WITH THE PLASMONIC SYSTEM “GRATING– 2D-GAS”. ANALYSIS OF FEATURES OF THE NEAR FIELD

PACS 85.60.-q, 07.57-c,
42.25.Bs, 42.79.Pw

The theory of interaction between electromagnetic waves and a plasmonic structure consisting of the subwavelength metal grating locating over the layer of a two-dimensional (2D) electron gas has been developed. The frequency dependences of the transmission, reflection, and loss coefficients are shown to have a resonant behavior relating to the excitation of plasmons in the 2D gas. The influence of the geometrical and electrical parameters of the system on the plasmon resonance characteristics is studied, and the structure of an electromagnetic field in the near-field zone is analyzed. The spatial distributions of the electric field components, the electric power density, and the electromagnetic wave polarization are found. The plasmon resonance is shown to substantially increase the local concentration of the electric field in the near-field zone of the grating.

Keywords: grating, near field, near-field zone, plasmonic system/structure, transmission, reflection, and loss coefficients, strip, circularly/elliptically polarized.

1. Introduction

Nowadays, the progress in modern micro- and optoelectronics is associated with the development of elements – generators, detectors, modulators – active in the terahertz (THz) range of electromagnetic radiation. The generators and detectors available today for this frequency range have a number of shortcomings. These are a low efficiency, the lack of the opportunity to continuously vary the operating frequency, a high price, and so on, which makes their wide application problematic [1]. One of the promising directions in the further exploitation of the THz frequency range seems to consist in creating the active elements operating on the basis of the excitation of electron gas oscillations in plasmonic semiconductor structures [2–6]. The modern field-effect transistor is the simplest example of this structure, in which the gate plays the role of a specific antenna element that allows the long-wave THz radiation to be coupled with short-wave plasmon oscillations of electrons in the transistor channel. In particular, a possibility of the terahertz plasmon detecting on the basis of single- [7, 8] and multigate [4, 6, 9, 10] transistor structures was demonstrated experimentally.

Multigate transistor structures are regarded to be promising candidates for the creation of active elements in generators with electric pumping and high-effective detectors of THz radiation. For such structures, the theories of THz radiation amplification [11, 12] and detecting [13, 14] were built. In particular, an approach to solve the Maxwell equations for the “metal grating–two-dimensional electron gas” structure was elaborated and used as a basis to calculate the corresponding transmission, reflection, absorption, emission, and photoresponse spectra in the THz frequency range.

However, a detailed analysis of the electromagnetic field structure in the near-field zone of the system remained beyond the scope of consideration in those works. At the same time, as was shown in our work [15], the electromagnetic field in the near-field zone of a single metal grating (hereafter, grating) has a number of peculiarities. In particular, the electromagnetic field becomes strongly concentrated near the edges of metal strips, and the polarization characteristics of the structure are strongly non-uniform in space. This work continues our previous researches. Here, we consider the interaction of an electromagnetic wave with the “grating–two-dimensional (2D) electron gas” system and focus attention on studying the near-field structure. The analysis of the near-field geometry in

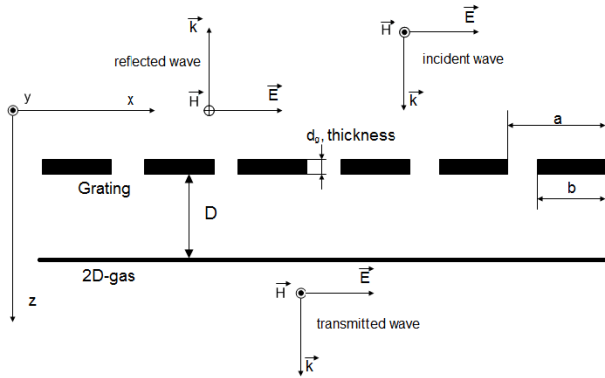


Fig. 1. Schematic diagram of the grating-2D gas structure

plasmonic structures also turns out challenging in view of the results of the newest researches concerning *hybrid* plasmonic structures intended to be used for studying the dynamics of individual molecules or nanoparticles, and the features of their radiation emission/absorption characteristics in vicinities of metal objects and structures [16–19].

The structure of this work is as follows. The electrodynamic theory of interaction between a plane electromagnetic wave and a grating-2D gas system is presented in brief in Section 2. The peculiarities in the THz radiation transmission, reflection, and absorption spectra and their relation to plasmon excitations in the 2D gas are considered in Section 3. The features in the spatial distributions of electric components, energy density, and polarization characteristics of the electromagnetic field in the near-field zone of the grating-2D gas system are discussed in Section 4. The main conclusions of the work are made in Section 5.

2. Electrodynamic Theory of the Grating-2D Gas System

In order to calculate the electrical and optical characteristics of the grating-2D gas system, let us take advantage of the approach developed in works [11, 15, 20]. Consider a structure consisting of a grating and a 2D gas (Fig. 1) and a plane electromagnetic wave, $\mathbf{E}_0 \exp(-i\omega t)$, incident on it. Let the wave fall normally to the grating plane, and let its polarization vector be directed along the grating axis (axis OX). We consider the grating period a to be much smaller than the wavelength λ of incident radiation. We suppose also that the thickness of grating's metal strips,

d_g , is much narrower than the thickness of a skin-layer at the incident-wave frequency ω , so that the inequality $d_g \ll c/\sqrt{2\pi\sigma_g\omega}$ is obeyed, where c is the light speed, and σ_g is the uniform bulk conductivity of the metal which the strips are made of. This assumption allows the grating to be considered as a two-dimensional periodic structure described by the conductivity $\sigma(x, z) = \sigma^G(x)\delta(z)$. The strip conductivity profile, $\sigma^G(x)$, will be considered below.

The total electric field \mathbf{E} obtained as a result of the interaction between the incident wave and the grating-2D gas structure satisfies the Maxwell equation

$$\text{rot rot } \mathbf{E}(\mathbf{r}, t) + \frac{\epsilon}{c^2} \frac{\partial \mathbf{E}(\mathbf{r}, t)}{\partial t^2} = -\frac{4\pi}{c^2} \frac{\partial \mathbf{j}(\mathbf{r}, t)}{\partial t}, \quad (1)$$

where $\mathbf{j}(\mathbf{r}, t)$ describes currents induced by the field in the grating strips and the 2D gas; and ϵ is the dielectric permittivity of the medium, in which the system is located. Since the system is uniform along the OY axis, the resulting electromagnetic field in the near-field zone is of the H -type, i.e. its nonzero components are $E_x(x, z)$, $E_z(x, z)$, and $H_y(x, z)$ [21]. The periodic character of a grating along the OX axis allows the solution of Eq. (1) to be sought in the form of a Fourier series

$$E_{\{x,z\}} = \sum_{m=-\infty}^{+\infty} E_{\{x,z\}}^{(m)}(z) \exp(iq_m x), \quad (2)$$

where $q_m = 2\pi m/a$ is the reciprocal lattice vector of the grating, and m are integers. After substituting formula (2) into Eq. (1), we obtain the following system of ordinary differential equations for the Fourier components of the electric field,

$$\begin{aligned} \frac{\partial^2 E_x^{(m)}}{\partial z^2} - k_m^2 E_x^{(m)} &= \\ &= \frac{4\pi i k_m^2}{\epsilon \omega} \left(j_x^{(m),G} \delta(z) + j_x^{(m),2D} \delta(z-D) \right), \quad (3) \\ E_z^{(m)} &= -i \frac{q_m}{k_m^2} \frac{\partial E_x^{(m)}}{\partial z}. \end{aligned}$$

At $a < m\lambda_0$, the wave number $k_m = \sqrt{q_m^2 - \epsilon\omega^2/c^2}$ describes evanescent modes of the near field, and, at $a > m\lambda_0$, the wave number $k_m = -i\sqrt{\epsilon\omega^2/c^2 - q_m^2}$ describes non-local modes in the far-field zone. The quantities $j_x^{(m),G}$ and $j_x^{(m),2D}$ are the Fourier components of currents induced by the external field in the

grating and the 2D gas, respectively. In the linear approximation, according to the Ohm law, the Fourier components of those currents can be expressed in terms of the field components $E_x^{(m)}$ as follows:

$$\begin{aligned} j_x^{(m),G} &= \sum_{m'=-\infty}^{\infty} \sigma_{m-m'}^G E_x^{(m')}|_{z=0}, \\ j_x^{(m),2D} &= \sigma^{2D} E_x^{(m)}|_{z=D}. \end{aligned} \quad (4)$$

The Fourier components of the grating conductivity, σ_m^G , depend on the geometrical profile of the strip conductivity, $\sigma^G(x)$; namely,

$$\sigma_m^G(\omega) = \int_0^a \sigma^G(x) \exp(-iq_m x) \frac{dx}{a}.$$

Analogously to what was done in the previous work [15], we use a smoothed profile to describe the metal strips of the grating,

$$\sigma^G(x) = \sigma_g d_g \begin{cases} \sin^p(\pi x/b), & x \in [0, b] \\ 0, & x \in [b, a], \end{cases} \quad (5)$$

where b is the strip width. In this work, we use the value $p = 1/6$. It is worth noting that the smoothing procedure for the conductivity profile in the strips (formula (5)) allowed us to obtain a quicker convergence for series (2) in comparison with the case of a step-like profile. In all following calculations, we assumed that there is no frequency dispersion for the strip metal, and that the frequency dispersion for the 2D gas is described by the Drude–Lorentz model with the effective momentum relaxation time for electrons τ ,

$$\sigma^{2D} = \sigma_0^{2D} / (1 - i\omega\tau). \quad (6)$$

The solution of system (3) has to satisfy the continuity condition for the component $E_x^{(m)}$ across the grating and 2D-gas planes,

$$E_x^{(m)}|_{z=+0, D+0} = E_x^{(m)}|_{z=-0, D-0}, \quad (7)$$

as well as the condition of a derivative jump,

$$\begin{aligned} \left. \frac{\partial E_x^{(m)}}{\partial z} \right|_{z=+0, D+0} - \left. \frac{\partial E_x^{(m)}}{\partial z} \right|_{z=-0, D-0} &= \\ &= \frac{4\pi i k_m^2}{\omega \epsilon} j_x^{(m), (G, 2D)}. \end{aligned} \quad (8)$$

Using Eqs. (3)–(8), the mathematical formulation of the electrodynamic problem for the grating–2D gas system can be reduced to a system of algebraic equations for the Fourier components $E_x^{(m)}$ in the grating plane,

$$\begin{aligned} \sum_{m'=-\infty}^{\infty} \left\{ \delta_{m, m'} + \frac{2\pi i k_m}{\epsilon \omega} W(m, \omega) \sigma_{m-m'}^G \right\} E_x^{(m')}|_{z=0} &= \\ &= W(m, \omega) \delta_{m, 0} E_0. \end{aligned} \quad (9)$$

Here, E_0 is the incident wave amplitude, and we use the notation

$$W(m, \omega) = 1 - (1 - 1/\epsilon_{2D}(m, \omega)) \exp(-2k_m D),$$

where $\epsilon_{2D}(m, \omega) = 1 + 2\pi i k_m \sigma^{2D}(\omega)/\omega \epsilon$.

The solution of system (9) gives the following formula for the electric field distribution in the whole space, including the near-field zone ($z \leq a$):

$$\begin{aligned} E_x(x, z) &= E_0 \exp\left(i \frac{\omega \sqrt{\epsilon}}{c} z\right) + \\ &+ \sum_{m=-\infty}^{\infty} \left(C_1^{(m)} \exp(-k_m |z|) + \right. \\ &\left. + C_2^{(m)} \exp(-k_m |z - D|) \right) \exp(iq_m x). \end{aligned} \quad (10)$$

Here, the constants $C_1^{(m)}$ and $C_2^{(m)}$ are expressed in terms of the Fourier coefficients $E_x^{(m)}|_{z=0}$ as follows:

$$C_1^{(m)} = \frac{E_x^{(m)}|_{z=0}}{W(m, \omega)} - E_0 \delta_{0, m}, \quad (11)$$

$$C_2^{(m)} = \left(1 - \frac{1}{W(m, \omega)} \right) E_x^{(m)}|_{z=0} \exp(k_m D). \quad (12)$$

Using constants (11) and (12), it is easy to obtain the distributions of the charge density and currents in the grating strips and the 2D gas,

$$\rho^{G, 2D}(x) = \sum_{m=-\infty}^{\infty} \frac{i\epsilon q_m}{2\pi k_m} C_{1,2}^{(m)} \exp(iq_m x), \quad (13)$$

$$j^{G, 2D}(x) = \sum_{m=-\infty}^{\infty} \frac{i\epsilon \omega}{2\pi k_m} C_{1,2}^{(m)} \exp(iq_m x). \quad (14)$$

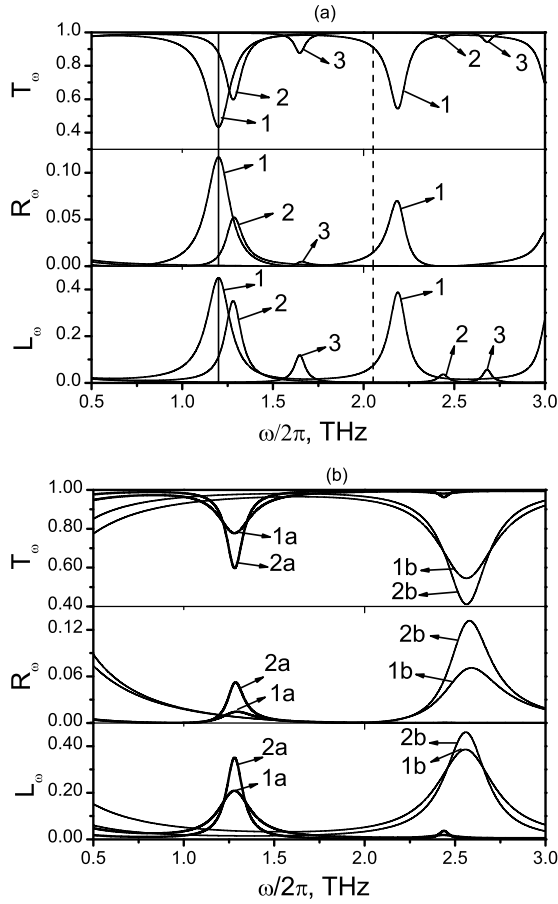


Fig. 2. Frequency dependences of the coefficients T_ω , R_ω , and L_ω . Panel (a) illustrates the influence of the grating filling factor $b/a = 0.9$ (1), 0.6 (2), and 0.3 (3). Calculation parameters are $\sigma_G = 4 \times 10^{15} \text{ s}^{-1}$, $d_g = 0.02 \text{ } \mu\text{m}$, $n^{2D} = 10^{12} \text{ cm}^{-2}$, and $\tau = 3.0 \text{ ps}$. Panel (b) demonstrates the influence of 2D gas parameters: (1a) $\tau = 1.0 \text{ ps}$, $n^{2D} = 10^{12} \text{ cm}^{-2}$; (1b) $\tau = 1.0 \text{ ps}$, $n^{2D} = 4 \times 10^{12} \text{ cm}^{-2}$; (2a) $\tau = 3.0 \text{ ps}$, $n^{2D} = 10^{12} \text{ cm}^{-2}$; and (2b) $\tau = 3.0 \text{ ps}$, $n^{2D} = 4 \times 10^{12} \text{ cm}^{-2}$. The grating filling factor $b/a = 0.6$

Note that the charge distribution (13) is determined by the jump of the electric field z -component, namely:

$$E_z|_{z=+0, D+0} - E_z|_{z=-0, D-0} = \frac{4\pi}{\epsilon} \rho^{G, 2D}. \quad (15)$$

Using the solution of system (9), it is easy to obtain the optical characteristics of the grating–2D gas system in the far-field zone ($z \gg a$), namely, to calculate the transmission, reflection, and loss coefficients. In the case of a subwavelength grating ($a < \lambda_0$), those coefficients depend only on the zeroth Fourier com-

ponent, $E_x^{(0)}$; namely,

$$T_\omega = \left| \frac{E_x^{(0)}|_{z=0}}{W(0, \omega)\epsilon(0, \omega)} \right|^2 / |E_0|^2, \quad (16)$$

$$R_\omega = \left| E_{x,0}(z)|_{z=0} - E_0 \right|^2 / |E_0|^2, \quad (17)$$

$$L_\omega = 1 - T_\omega - R_\omega. \quad (18)$$

Hence, formulas (10)–(18) allow the optical characteristics of the grating–2D gas system to be calculated in both the far- and near-field zones.

3. Frequency Dependences of the Transmission, Reflection, and Loss Coefficients

Let us analyze spectra of the transmission, T , reflection, R , and loss, L , coefficients for the grating–2D gas structure in the case where the parameters of a 2D gas correspond to a real material used in modern THz optoelectronics, gallium nitride (GaN). The researches of peculiarities in the optical characteristics of GaN-based heterostructures in the THz frequency range attracted a substantial attention, because this material is widely used while creating THz modulators and generators [22–24].

As is seen from Fig. 2, the T_ω , R_ω , and L_ω spectra have a resonant behavior: there exist a number of extrema in them, which correspond to the resonant absorption of electromagnetic waves by plasmons in the 2D gas. Plasmons are excited by oscillating charges induced by the incident wave in the grating strips (the excitation mechanism is discussed in Section 4 in more details). Actually, the grating plays the role of a connecting link between long-wave THz radiation and short-wave plasmon oscillations in the 2D gas.

As follows from Section 2, the resulting field in the grating–2D gas system is modulated with the spatial period equal to a . Therefore, the excited plasmons have wave vectors equal to or multiple of the reciprocal lattice vector of a grating. Since we deal with the 2D gas partially screened by metal strips, it is natural to expect that the characteristic absorption frequencies ω_s for the grating–2D gas system should fall within the interval between the plasmon frequencies of completely gated, $\omega_g = \sqrt{4\pi e^2 n^{2D} q / m^* \epsilon (\coth qD + 1)}$, and ungated, $\omega_{ng} = \sqrt{2\pi e^2 n^{2D} q / m^* \epsilon}$, 2D electron gases, where

$q = q_m$ ($m = 1, 2, 3, \dots$). (The expressions for the frequencies ω_g and ω_{ng} can be found, e.g., in work [2].)

In Fig. 2, *a*, the frequencies ω_g and ω_{ng} corresponding to the first resonance ($m = 1$) are marked by solid and dashed vertical lines, respectively. The values $\omega_g/2\pi = 1.2$ THz and $\omega_{ng}/2\pi = 2.1$ THz were obtained for the following parameters of the system: the 2D gas concentration $n^{2D} = 10^{12}$ cm $^{-2}$, the effective mass $m^* = 0.2m_e$, where m_e is the free electron mass, $\epsilon = 1$, the grating period $a = 3$ μ m, and the distance between the grating and the 2D gas $D = 0.1$ μ m.

The magnitudes of characteristic frequencies ω_s depend on the parameters of both the grating and the 2D gas. For instance, as the grating filling factor (the ratio b/a) decreases, the plasmon resonance frequencies shift toward higher values and gradually approach the frequency ω_g (curves 1 to 3); in addition, the intensity of resonances become greatly weakened until they practically disappear at $b/a < 0.3$. This dependence can be explained by the fact that a reduction of the filling factor is accompanied by a decrease of the near-field concentration in a vicinity of the grating strip edges [15]. From whence, it follows that a grating with narrow gaps between the strips provides a much better interaction between the plasmons and the external field. If the grating is absent ($b/a = 0$), the plane electromagnetic wave does not interact with plasmons, and the spectra of T_ω , R_ω , and L_ω coefficients for a single 2D gas with conductivity (6) have simple forms,

$$T_\omega^{2D} = \frac{\omega^2 + \gamma^2}{\omega^2 + (\Gamma + \gamma)^2},$$

$$R_\omega^{2D} = \frac{\Gamma^2}{\omega^2 + (\Gamma + \gamma)^2},$$

$$L_\omega^{2D} = \frac{2\Gamma\gamma}{\omega^2 + (\Gamma + \gamma)^2},$$

being determined only by the magnitudes of radiation, $\Gamma = 2\pi n^{2D} e^2 / m^* c \sqrt{\epsilon}$, and non-radiation, $\gamma = 1/\tau$, losses. The parameter Γ is the reciprocal time of the oscillation damping for charge carriers in the 2D gas emitting electromagnetic waves. For the parameters of the 2D gas given above, we obtain $\Gamma = 0.26$ ps $^{-1}$, $\gamma = 0.33$ ps $^{-1}$, $T_\omega^{2D} = 0.994$, $R_\omega^{2D} = 0.002$, and $L_\omega^{2D} = 0.004$ at a frequency of 1 THz.

The analysis of the dependences of plasmon resonance parameters on the parameters of the 2D gas, namely, the electron concentration and the electron

relaxation time τ , is presented in Fig. 1, *b*. One can see that a change of the relaxation time or the mobility of electrons does not affect the positions of resonances (curves 1, *a* and 2, *a*), but vary their half-widths and intensities. The growth of the electron mobility increases the Q-factor of plasmon oscillations, which results in a reduction of the resonance half-width and a simultaneous growth of the intensities at the extrema of the T_ω , R_ω , and L_ω dependences. At the same time, an increase of the electron concentration in the 2D gas is responsible for both the growth of resonance peaks (see, e.g., curves 1, *a* and 1, *b*) and their shift toward high frequencies in accordance with the formulas for ω_{ng} . If the concentration becomes four times higher (from $n^{2D} = 10^{12}$ cm $^{-2}$ to $n^{2D} = 4 \times 10^{12}$ cm $^{-2}$), the frequency of the resonance increases by a factor of two (from $\omega/2\pi = 1.25$ THz to $\omega/2\pi = 2.5$ THz). The increase of peak intensities (see curves 1*a* and 1*b*) can be explained, on the one hand, by a stronger interaction between the electromagnetic field and plasmon oscillations (the amplitudes of high-frequency currents excited in the 2D gas are proportional to the conductivity σ^{2D}). On the other hand, as the frequency increases, the Q-factor of plasmon oscillations also increases, provided that τ remains constant. The growth of electron concentration also gives rise to an increase of the resonance half-width, which is associated with the growth of radiation losses.

Hence, by changing the parameters of the grating and the 2D gas, we can excite plasmon oscillations and observe the resonant absorption of electromagnetic waves in a wide interval of THz frequencies.

4. Near-Field Structure in the Grating–2D Gas System

In the far-field zone of a subwavelength grating, the transmitted and reflected waves are planar, being formed by only the zeroth Fourier component $E_x^{(0)}$. At the same time, the electromagnetic field in the near-field zone of the system has a complicated vector structure formed by plenty of evanescent modes $E_{x,z}^{(m)}$. Here, the field distribution is a result of the superposition of two fields: a field generated by the incident wave and an induced field arising owing to the charge redistribution in the grating and the 2D gas.

We found that the electric charge distribution has structure of a quadrupole that oscillates at the fre-

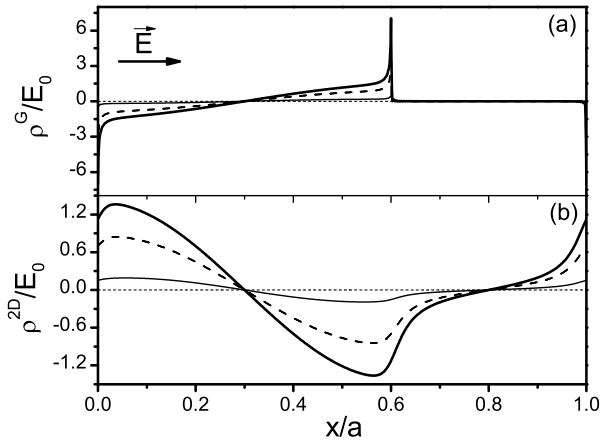


Fig. 3. Distributions of the two-dimensional induced charge density over the grating (a) and the 2D gas (b) at various time moments $t = 0$ (solid curve), $T/6$ (dashed curve), and $T/4$ (thin solid curve). The direction of the electric field of the incident wave at the time moment $t = 0$ is shown by an arrow. The parameter $\omega/2\pi = 1$ THz, and the other parameters of the system are the same as for curves 2 in Fig. 2, a

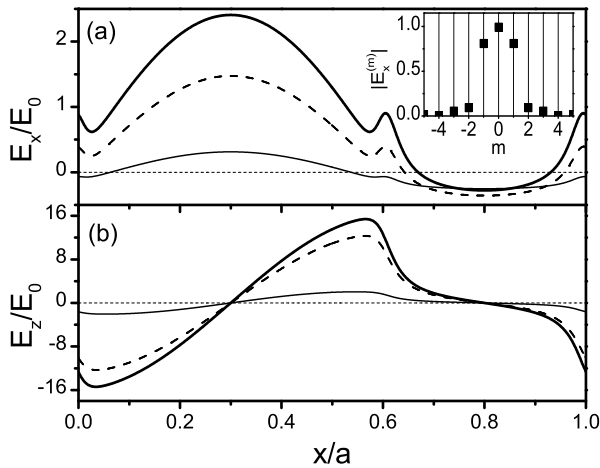


Fig. 4. Distributions of the electromagnetic wave field components (a) $E_x(x, z_0)$ and (b) $E_z(x, z_0)$ along the x -coordinate at $z_0 = 0.9D$ at various time moments $t = 0$ (solid curve), $T/6$ (dashed curve), and $T/4$ (thin solid curve). The parameter $\omega/2\pi = 1$ THz, and the other parameters of the system are the same as for curves 2 in Fig. 2, a

quency of the external signal. In Fig. 3, the distributions of the two-dimensional charge density at fixed time moments, which is normalized by E_0 , are depicted. Note that the two-dimensional charge density has the dimensionality of the field (see Eq. (15)). One

can see that the charge density on the grating is strongly non-uniform. The electric charge is concentrated very much near the edges of metal strips. As a result, the field is also strongly concentrated there. The charges induced on strips by the field of an incident wave, in turn, invoke a non-uniform distribution of the electron concentration in the 2D gas, and this distribution oscillates in antiphase with the grating charge. One should pay attention to that, owing to the symmetry of the system and its electroneutrality in general, there exist specific points, $x/a = 0.3$ and $x/a = 0.8$ (these are the middle points in the strip and in the gap between the strips, respectively), at which the induced charge equals zero. These points play the role of nodes for charge oscillations, which look like standing waves. Generally speaking, oscillations of any electric parameter along the OX axis look like standing waves in our problem, because there are no factors that would break the symmetry of the system with respect to the substitution $x \rightarrow -x$.

The oscillations of electric field components are illustrated in Fig. 4. The plots demonstrate that, at a given frequency of 1.0 THz, the x - and z -components reach the maximum at the initial time moment ($t = 0$), being almost in phase with the incident wave. Nevertheless, the field components have small phase shifts with respect to the incident wave. At the time moment $t = T/4$, the incident wave field vanishes, whereas the total field in the near zone does not (thin solid curves). The amplitudes of electric field oscillations are strongly different in the regions under the grating strip ($0 < x < b$) and between the strips ($b < x < a$). The z -component of the field mainly dominates in the interval $0 < x < b$. At the same time, the x -component dominates in the inter-strip gap $b < x < a$, except for the regions near the strip edges. For the z -component of the field, as well as for the charge oscillations, there are node points, at which $E_z = 0$. This is in contrast to the field x -component, for which the nodes are absent. However, the Fourier spectrum of E_x -oscillations is symmetric with respect to $m = 0$ (see the inset in Fig. 4, a). It should be noted that approximately five evanescent modes form the field structure near the 2D gas.

From Fig. 5, a, one can see that the profiles of the x -component along the axis OX strongly differ from one another depending on the coordinate z . Near the grating ($z = 0.2D$, thick solid curve), the component E_x has the same features as in the case of a single

grating, namely, a minimum in the interval screened by the metal strip, and strongly pronounced maxima near the strip edges [15]. When moving away from the grating, those maxima are rapidly smeared owing to the influence of charges induced in the 2D gas (dashed and thin solid curves). There emerges a maximum in the interval under the metal strip and a minimum under the gap, the amplitudes of the both grow when approaching the 2D gas. Since the charges induced in the 2D gas are opposite by sign to the charges in the strip, the field generating by the 2D gas compensates the grating-induced field along the axis OX and even can prevail when approaching the 2D gas plane. This fact qualitatively explains the changes in the field structure depending on the coordinate z .

Unlike the E_x component, the E_z one (Fig. 5, *b*) practically is not changed, as the coordinate z varies. This constancy is associated with the fact that a reduction of the E_z component of the grating field at larger distances is compensated by a growth of the field generated by the charges induced in the 2D gas (while approaching the latter). Qualitatively, this field distribution reminds that in a plane capacitor, for which the metal grating strip and the layer of 2D gas beneath play the role of its plates, between which the E_z component of the field is concentrated (the capacitor effect). The amplitude of the E_z component reaches a much larger value in this case than the amplitude of the E_x component. Despite that the E_z component is uniformly distributed along the axis OZ , its distribution along the axis OX remains strongly non-uniform. This is the essence of the difference between the electric field distributions in the grating–2D gas system and in the plane capacitor.

4.1. Distribution of the energy density of the electric field in the near-field zone of the grating–2D gas system

As a result of the capacitor effect giving rise to the concentration of the electric field, a strong local concentration of the electromagnetic field energy takes place in the grating–2D gas system in the region between its components. This phenomenon is illustrated by two-dimensional maps illustrating the spatial distribution of the electric field energy density averaged over the period (Fig. 6). The energy density maps were plotted for the dimensionless quantity $W(x, z)$ normalized by the energy density in the incident wave

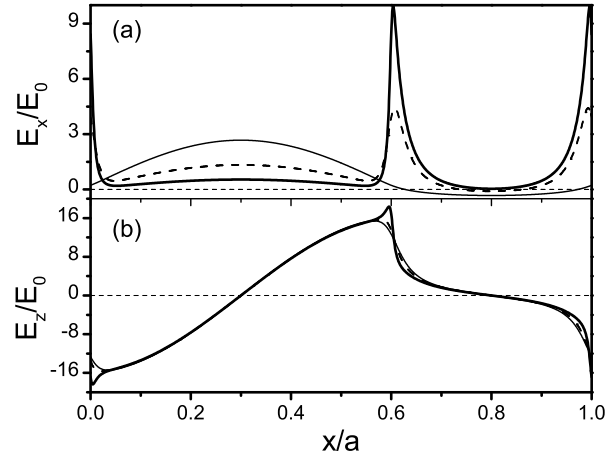


Fig. 5. Distributions of the electromagnetic wave field components (a) $E_x(x, z_0)$ and (b) $E_z(x, z_0)$ at various distances from the grating $z_0 = 0.2D$ (thin solid curve), $0.5D$ (dashed curve), and $0.99D$ (thick solid curve) and at the same time moment. The parameter $\omega/2\pi = 1$ THz, and the other parameters of the system are the same as for curves 2 in Fig. 2, *a*

and determined as follows:

$$W(x, z) = (|E_x(x, z)|^2 + |E_z(x, z)|^2)/|E_0|^2.$$

For a single grating (panel *a*), the regions, where the energy is strongly concentrated, are localized under the grating gaps, and the maximum values $W(x, z) \sim 100$ are reached near the strip edges. At the same time, in the case of the grating–2D gas system, the situation is inverse (panel *b*); namely, the near-field energy is mainly concentrated in the regions under the grating strips, where the z -component of the field dominates. The corresponding energy density reaches values of the order of thousands. A strong dependence of the patterns describing the energy density distribution in the grating–2D gas system on the incident wave frequency should also be marked; this dependence is almost not observed for a single grating. In panel *b*, the frequencies were so chosen to demonstrate the changes in the distribution of the electric field energy density when the system crosses the range of the plasmon resonance. In particular, a frequency of 1.0 THz corresponds to the subresonance range, a frequency of 1.25 THz frequency to the first plasmon resonance, and a frequency of 4 THz to the range above the first resonance. One can see that, in the case of the plasmon resonance (the middle map in panel *b*), the energy density in the near field con-

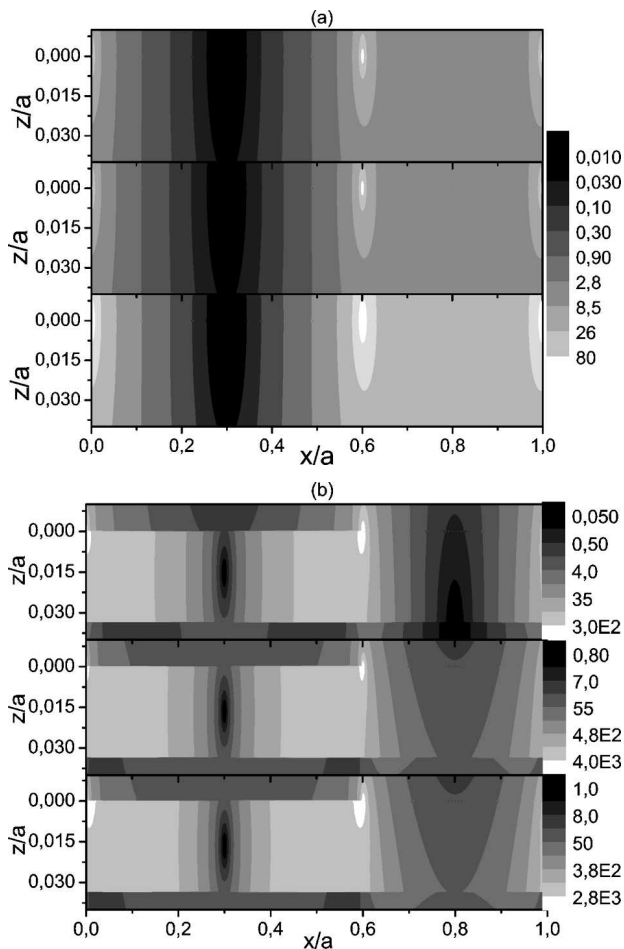


Fig. 6. Spatial distributions of the electric field energy density $W(x, z)$ (a) in a single grating and (b) in the grating–2D gas system at various frequencies of external electromagnetic wave: 1.0 (upper panel), 1.25 (the resonance frequency, middle panel), and 1.4 THz (lower panel). The parameters of the systems are the same as for curves 2 in Fig. 2, a

siderably increases in comparison with non-resonance frequencies.

We should emphasize the qualitative character of differences in the energy density distributions when changing from the single grating to the grating–2D gas system. The energy distribution reflects a dipole structure of the near field in the case of a single grating and its quadrupole structure in the case of the grating–2D gas system. The latter pattern can be illustrated by the presence of a *cold zone* in a vicinity of the quadrupole center, where the fields created by four charges are mutually compensated. If the distance D between the 2D gas and the grat-

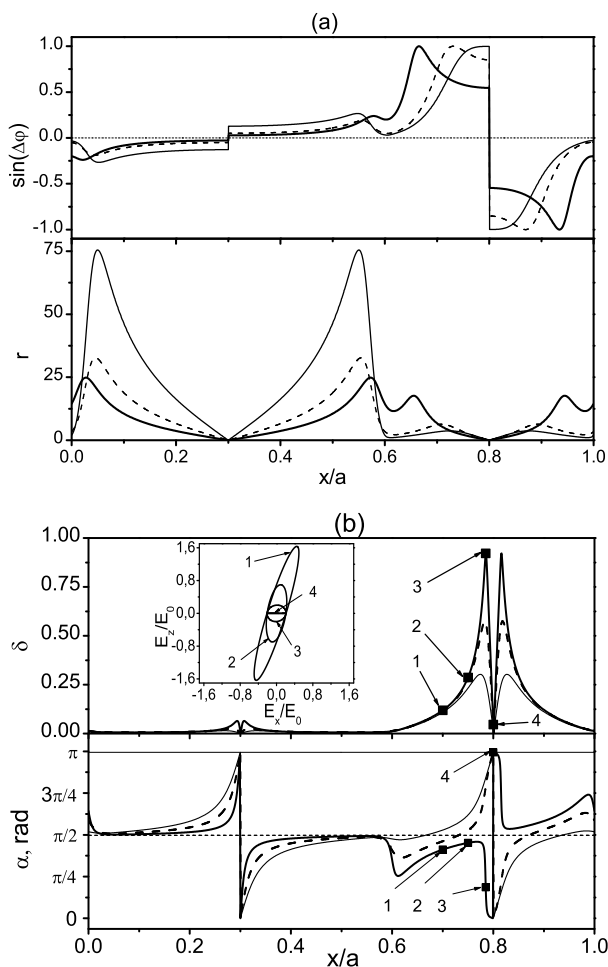


Fig. 7. Dependences (a) of the quantities $\sin(\Delta\varphi)$ (upper panel) and r (lower panel) and (b) of the ellipticity (upper panel) and the angle of the polarization ellipse slope (lower panel) on the coordinate x within the grating period at various distances from the grating $z = 0.2D$ (thick solid curves), $0.5D$ (dashed curves), and $0.9D$ (thin solid curves). The set of polarization ellipses corresponding to points 1 to 4 is shown in the inset. The signal frequency is 1 THz

ing is considerably shorter than the period a , the energy density distribution is formed, to a large extent, by the field component E_z . Since this component has breaks across the grating and the 2D gas, the quantity $W(x, z)$ also has well pronounced breaks across the grating plane (at $z/a = 0$) and the 2D gas plane (at $z/a = 0.033$). Hence, the spatial scale of the near-range field in the grating–2D gas system is determined by the distance D . In the case of a single grating, the grating period a plays the role of this scale.

4.2. Polarization properties of the near field

As was shown in the previous sections, when a plane electromagnetic wave interacts with a metal grating, the resulting electromagnetic field in the near-field zone has a complicated vector structure that includes two components of the electric field. Since the amplitudes and oscillation phases of those components are different from each other and strongly depend on the coordinates, it is possible to say that the electromagnetic wave in the near-field zone becomes elliptically polarized locally; i.e., within the oscillation period, the total field vector does not pass a straight line, but circumscribes an ellipse, the parameters of which are determined by the ratio between the absolute values of those components, $r = |E_z|/|E_x|$, and the phase shift $\Delta\varphi$ between them. This polarization ellipse is convenient to be characterized by the following parameters: the ellipticity δ is the ratio between the lengths of the minor and major semiaxes, and the azimuthal angle α is the angle between the major axis of the ellipse and the coordinate axis OX . The parameters of the polarization ellipse locally depend on the coordinates and are determined in terms of the parameters r and δ as follows (see work [25]):

$$\delta = \left[\frac{1 - \sqrt{1 - \beta^2}}{1 + \sqrt{1 - \beta^2}} \right],$$

$$\tan \alpha = \left[\frac{2r^2 - (1 + r^2)(1 - \sqrt{1 - \beta^2})}{2r \cos(\Delta\varphi)} \right],$$

where $\beta = 2r \sin(\Delta\varphi)/(1 + r^2)$.

Using those formulas, one can easily derive the corresponding expressions for the limiting cases of circular and linear electromagnetic wave polarizations. In particular, the circular polarization ($\delta = 1$, and $\tan \alpha$ is indefinite) is realized in the case where $\beta = 1$, for which $r = 1$ and $\Delta\varphi = \pi/2$. At the same time, the linear polarization ($\delta = 0$) corresponds to the case $\beta = 0$, which can take place either if $r = 0$ or ∞ (so that $\tan \alpha = 0$ or ∞ , respectively) or if $\Delta\varphi = 0$ or π (in this case, $\tan \alpha = \pm r$).

The typical dependences of the parameters δ and α on the coordinate x are exhibited in Fig. 7, *b*. For illustration, panel *a* demonstrates how the electromagnetic field parameters r and $\sin(\Delta\varphi)$ change as the coordinate varies. One can see that the electromagnetic wave is almost linearly polarized under the grating strip ($0 < x/a < 0.6$), because the absolute value of component E_z , $|E_z|$, considerably exceeds the absolute value of component E_x , $|E_x|$, with those

field components oscillating almost in phase (the upper plot in panel *a*). Almost in the whole region, the ellipticity does not exceed 0.02, and the azimuthal angle is close to $\pi/2$, except for a small interval under the middle of the strip, where the component $E_z \rightarrow 0$, and $r \rightarrow 0$. In the gap region $0.6 < x/a < 1$, the near-field geometry quickly varies, because the oscillation amplitudes of field components become comparable here, and the phase shift between them changes drastically. In the region $0.6 < x/a < 0.8$, the linearly polarized wave transforms into a substantially elliptical one (the set of polarization ellipses is shown in the inset in panel *b*). Near the characteristic point $x/a \approx 0.8$, which is the gap middle point, $E_z \rightarrow 0$, and the wave becomes linearly polarized. Further, at $0.8 < x/a < 1$, it becomes elliptically polarized again. While crossing the characteristic point $x/a = 0.8$, the azimuthal angle jumps from 0 to π , which corresponds to the sign change of the field z -component.

Information on the near field polarization can be important for the selective excitation of molecules or nanoobjects in hybrid plasmonic structures. Of special importance is the case where the excitation mechanisms depend not only on the intensity, but also on the direction of the field.

5. Conclusions

In this work, the interaction between a plane terahertz electromagnetic wave and a plasmonic structure “subwavelength metal grating–2D electron gas” has been studied. The behavior of the transmission, reflection, and loss coefficients has been analyzed, as well as the features in the near-field distribution. It is shown that the frequency dependences of the T , R , and L coefficients in the THz range reveal a number resonant extrema, which are associated with the excitation of plasmons in the 2D gas. Depending on the filling factor for the metal grating and the parameters of a 2D gas, the frequency and the intensity of plasmon resonances change. The growth of the filling factor results in an increase of the intensity of plasmon resonances and a reduction of their frequencies. The increase of the electron relaxation time in the 2D-gas channel does not affect the positions of resonances, but diminishes their half-widths owing to the growth of the Q-factor for plasmon oscillations. An increase of the electron concentration in the 2D gas is accompanied by an increase of the frequency and the half-

width of plasmon resonances. The near field of the system is shown to have a quasiquadrupole structure, which is a result of the excitation of opposite charges at the edges of grating strips by the incident wave and the specular image of those charges in the 2D gas plane. While considering the near field, the effects of local concentration and electric field amplification are shown to be considerably larger in comparison with those for a single metal grating. Moreover, at frequencies close to the plasmon resonance, those effects can grow further by an order of magnitude. It is also worth noting that the electric field in the near-field zone becomes concentrated in the interval between the metal strip of the grating and the region of the 2D gas under it.

Therefore, the application of the plasmonic system with subwavelength sizes provides its effective interaction with electromagnetic waves and enables a control over the radiation polarization and the concentration of the electromagnetic energy. Those features of the plasmonic system can be used to study the THz properties of low-dimensional charge carriers [26–28], to excite individual molecules in hybrid plasmonic systems [16–19], and to manipulate atomic states in systems with quantum qubits [29].

The work was supported by a joint project of NASU and RFBR.

1. M. Tonouchi, *Nature Photon.* **1**, 97 (2007).
2. A.V. Chaplik, *Surf. Sci. Rep.* **5**, 289 (1985).
3. M.I. Dyakonov, *CR Acad. Sci. B Phys.* **11**, 413 (2010).
4. T. Otsuji *et al.*, *J. Phys.: Condens. Matter* **20**, 384206 (2008).
5. V.V. Popov, *J. Infrared Milli. Terahz Wav.* **32**, 1178 (2011).
6. W. Knap, M. Dyakonov, D. Coquillat *et al.*, *J. Infrared Milli. Terahz Wav.* **30**, 1319 (2009).
7. D. Veksler, F. Teppe, A.P. Dmitriev, V.Yu. Kachorovskii, W. Knap, and M.S. Shur, *Phys. Rev. B* **73**, 125328 (2006).
8. M. Sakowicz, M.B. Lifshits, O.A. Klimenko, F. Schuster, D. Coquillat, F. Teppe, and W. Knap, *J. Appl. Phys.* **110**, 054512 (2011).
9. T. Watanabe, S.B. Tombet, Y. Tanimoto *et al.*, *Solid State Electron.* **78**, 109 (2012).
10. A.R. Davoyan, V.V. Popov, and S.A. Nikitov, *Phys. Rev. Lett.* **108**, 127401 (2012).
11. S.A. Mikhailov, *Recent Res. Devel. Appl. Phys.* **2**, 65 (1999).
12. S.A. Mikhailov, *Phys. Rev. B* **58**, 1517 (1998).
13. V.V. Popov, D.V. Fateev, T. Otsuji, Y.M. Meziani, D. Coquillat, and W. Knap, *Appl. Phys. Lett.* **99**, 3504 (2011).
14. G.R. Aizin, V.V. Popov, and O.V. Polischuk, *Appl. Phys. Lett.* **89**, 143512 (2006).
15. Yu.M. Lyaschuk and V.V. Korotyyev, *Ukr. J. Phys. Opt.* **13**, 142 (2012).
16. A. Trugler and U. Hohenester, arXiv: 0802.1630 (2008)
17. J.R. Lakowicz, K. Ray, M. Chowdhury, H. Szmecinski, Y. Fu, J. Zhang, and K. Nowaczyk, *Analyst* **133**, 1308 (2008).
18. G. Baffou, C. Girard, E. Dujardin, G.C. des Francs, and O.J.F. Martin, *Phys. Rev. B* **77**, 121101 (2008).
19. V.A. Kochelap and S.M. Kukhtaruk, *J. Appl. Phys.* **109**, 114318 (2011); *Ukr. J. Phys.* **57**, 367 (2012).
20. R. Petit, *Nouv. Rev. Opt.* **6**, 129 (1975).
21. M. Born and E.W. Wolf, *Principles of Optics: Electromagnetic Theory of Propagation, Interference and Diffraction of Light* (Cambridge Univ. Press, Cambridge, 1999).
22. T. Laurent, R. Sharma, J. Torres, P. Nouvel, S. Blin, L. Varani, Y. Cordier, M. Chmielowska, S. Chenot, J.-P. Faurie, B. Beaumont, P. Shiktorov, E. Starikov, V. Gruzinski, V.V. Korotyyev, and V.A. Kochelap, *Appl. Phys. Lett.* **99**, 082101 (2011).
23. G.I. Syngayivska and V.V. Korotyyev, *Ukr. J. Phys.* **58**, 40 (2013).
24. G.I. Syngayivska, V.V. Korotyyev, and V.A. Kochelap, *Semicond. Sci. Technol.* **28** 035007 (2013).
25. V.V. Korotyyev, *Semicond. Phys. Quant. Electr. Optoelectr.* **16**, 18 (2013).
26. V.N. Sokolov, K.W. Kim, V.A. Kochelap, and D.L. Woolard, *Appl. Phys. Lett.* **84**, 3630 (2004).
27. V.V. Korotyyev, V.A. Kochelap, A.A. Klimov, K.W. Kim, and D.L. Woolard, *J. Appl. Phys.* **96**, 6488 (2004).
28. J. Lloyd-Hughes and T.-I. Jeon, *J. Infrared Milli. Terahz Wav.* **33**, 871 (2012).
29. *Quantum Coherence and Information Processing*, edited by D. Esteve, J.M. Raimond, and J. Dalibard (Elsevier, London, 2004).

Received 21.05.2013.

Translated from Ukrainian by O.I. Voitenko

Ю.М. Ляшук, В.В. Коротеев

ВЗАЄМОДІЯ ТЕРАГЕРЦОВОЇ ЕЛЕКТРОМАГНІТНОЇ ХВИЛІ З ПЛАЗМОННОЮ СИСТЕМОЮ “МЕТАЛІЧНА ГРАТКА – ЕЛЕКТРОННИЙ 2D-ГАЗ”. АНАЛІЗ ОСОБЛИВОСТЕЙ БЛИЖНЬОГО ПОЛЯ

Резюме

В роботі представлена теорія взаємодії електромагнітних хвиль з плазмонною системою, що складається з субхвильової металічної ґратки та шару електронного 2D-газу, розміщеного під нею. Показано, що частотні залежності коефіцієнтів пропускання, відбивання та втрат такої системи мають особливості, пов'язані зі збудженням плазмонів в 2D-газі. Досліджено вплив геометричних та електричних параметрів системи на характеристики плазмонного резонансу. Проаналізовано структуру електромагнітного поля в ближній зоні системи. Знайдено просторові залежності електричних компонент, густини електричної енергії та поляризації. Показано, що плазмонний резонанс істотно збільшує локальну концентрацію електромагнітного поля в ближній зоні ґратки.